LA-UR- 93-1470

Title: ION ANISOTROPY DRIVEN WAVES IN THE EARTH'S MAGNETOSHEATH AND PLASMA DEPLETION LAYER

Author(s): R.E. Denton, B.J. Anderson, S.A. Fuselier, S.P. Gary, and M.K. Hudson

Submitted to: 1993 Yosemite Conference on Space Plasmas, Yosemite, CA,

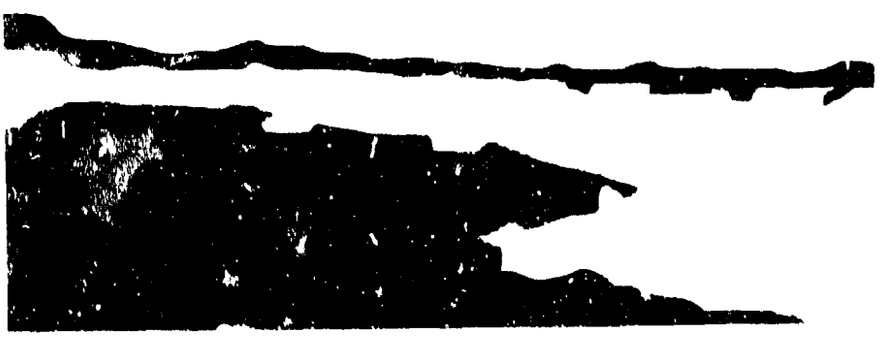

Los Alamos
NATIONAL LABORATORY

Ion Anisotropy Driven Waves in the Earth's Magnetosheath and Plasma Depletion Layer

RICHARD E. DENTON

Physics and Astronomy Dept., Dartmouth College, Hanover, NH 03755-3528

BRIAN J. ANDERSON

Applied Physics Laboratory, Johns Hopkins Univ., Laurel, MD 20723-6099

STEPHEN A. FUSELIER

Lockheed Palo Alto Research Laboratory, Palo Alto, CA 94304

S. P. GARY

Los Alamos National Laboratory, Los Alamos, NM 87545

MARY K. HUDSON

Physics and Astronomy Dept., Dartmouth College

Recent studies of low frequency waves ($\omega_r \lesssim \Omega_p$, where Ω_p is the proton gyrofrequency) observed by AMPTE/CCE in the plasma depletion layer and magnetosheath proper are reviewed. These waves are shown to be well identified with ion cyclotron and mirror mode waves. By statistically analyzing the transitions between the magnetopause and time intervals with ion cyclotron and mirror mode waves, it is established that the regions in which ion cyclotron waves occur are between the magnetopause and the regions where the mirror mode is observed. This result is shown to follow from the fact that the wave spectral properties are ordered with respect to the proton parallel beta, $\beta_{\parallel p}$. The later result is predicted by linear Vlasov theory using a simple model for the magnetosheath and plasma depletion layer. Thus, the observed spectral type can be associated with relative distance from the magnetopause. The anisotropy beta relation, $A_p = (T_\perp/T_\parallel)_p - 1 = 0.50/\beta_{\parallel p}^{0.48}$ results from the fact that the waves pitch angle scatter the particles so that the plasma is near marginal stability, and is a fundamental constraint on the plasma

DISCLAIMER

INTRODUCTION

The plasma depletion layer [*Crooker et al.*, 1979; *Midgley and Davis*, 1963; *Lees*, 1964; *Zwan and Wolf*, 1976; *Wu*, 1992] is a relatively thin layer ($\approx 0.5\mathcal{R}_E$ thick, where $\mathcal{R}_E$ is the radius of the Earth) which forms on the sunward side of the magnetopause in the subsolar region when the Interplanetary Magnetic Field (IMF) is quasi-perpendicular (at a large angle) to the Earth-Sun line, that is, roughly tangent to the subsolar magnetopause. Magnetic flux from the magnetosheath is compressed as it convects through the plasma depletion layer and presses against the magnetopause; at the same time, the plasma density is depleted. The combined effect of increased magnetic field strength, B_0, and depleted density is that the plasma beta is greatly reduced at the magnetopause edge of the plasma depletion layer compared to that in the magnetosheath proper (that region of the magnetosheath excluding the plasma depletion layer).

In the magnetosheath downstream of the quasi-perpendicular bow shock, the proton and doubly ionized helium species (alpha particles) often may be characterized approximately by bi-Maxwellian distributions with $T_\perp > T_\parallel$ [Sckopke et al., 1990; *Anderson et al.*, 1991; *Fuselier*, 1992]. Linear Vlasov theory predicts in this case the existence of three instabilities. The first two are the proton cyclotron and alpha cyclotron instabilities driven by the temperature anisotropies of the protons and alphas respectively and with real frequencies, ω_r, below their respective gyrofrequencies [*Gary et al.*, 1993a; *Denton et al.*, 1993a]. The third instability is the mirror mode at much lower ω_r [*Gary et al.*, 1976]. The ion cyclotron waves are transverse, that is, the fluctuating magnetic field, $\tilde{\mathbf{B}}$, is perpendicular to $\mathbf{B_0}$, while the mirror mode is compressional, with $\tilde{\mathbf{B}} \parallel \mathbf{B_0}$.

The AMPTE/CCE spacecraft passes through the magnetosheath under conditions such that the solar wind dynamic pressure is high, so that the magnetosheath beta is high, the magnetosphere is compressed, and the magnetopause lies within the AMPTE/CCE apogee of 8.8 R_E. Using the AMPTE/CCE data set, Anderson and Fuselier [1993] and Anderson et al. [1993] have shown that the spectral properties of observed low frequency waves (0.1 – 0.1 Hz, corresponding to ω_r less than the proton gyrofrequency, $\Omega_p = eB_0/m_pc$) are correlated with the variation of plasma parameters across the plasma depletion layer and into the magnetosheath proper. An example illustrating this correlation is shown in Figure 1. On October 18 (day 292), 1984, the AMPTE/CCE spacecraft crossed the subsolar magnetopause at a time during which the compan

ion spacecraft AMPTE/IRM and UKS were upstream of the bow shock in the solar wind. Because of this, it was possible to determine conclusively that changes in density and field strength in the vicinity of the magnetopause resulted from a crossing of the plasma depletion layer, as distinct from temporal changes in solar wind conditions [*Fuselier et al.*, 1991]. Figure 1 (adapted from [*Anderson and Fuselier*, 1993] and [*Fuselier et al.*, 1991]) shows dynamic spectra of AMPTE/CCE magnetic field data together with CCE and IRM density and magnetic field data. The top panel (labeled "XY") shows the transverse (to $\mathbf{B_0}$) spectral power from 0 to 2 Hz and the second panel (labeled "Z") shows the parallel power over the same frequency range. The third panel shows the electron density at CCE, calculated as the sum of the proton density and twice the He^{2+} density measured by the Hot Plasma Composition Experiment on CCE. The IRM electron density, measured by the electron instrument was multiplied by 4.92, determined as the ratio of the IRM and CCE densities from 1340 to 1400 UT. The IRM time has been shifted by 3.5 minutes to account for the plasma *convection* from IRM to CCE. This time was determined as discussed by Fuselier et al. [1991]. The bottom panel shows the CCE and IRM magnetic field strength, B_0. The IRM magnetic field magnitude was multiplied by 4.81, the ratio of the average IRM and CCE field magnitudes from 1340–1400 UT. The absolute density and magnetic field values are quite different upstream of the bow shock and close to the magnetopause; the shift in IRM values is made so that a relative comparison can be made. It is clear that the CCE and IRM densities are correlated during the interval 1340–1400, but not beforehand.

From 1300 to 1340 UT the CCE density is low and the CCE field strength is high relative to the values at IRM immediately upstream in the solar wind. As discussed by Fuselier et al. [1991] and Anderson et al. [1993], the CCE spacecraft was generally located in the magnetosheath after a magnetopause crossing at ~ 1300 UT. Comparison with the upstream solar wind monitor indicates that the interval from 1303 to 1340 UT has characteristics of a plasma depletion layer since the density is depleted and the field strength enhanced at CCE relative to IRM. The correspondence of this interval with the transverse magnetic signals (top panel of Figure 1) indicative of ion cyclotron waves is clear, as is the progressive intensification of low frequency compressional fluctuations (second panel) after 1330 UT. We identify the latter as mirror mode fluctuations. We will show below that these mode identifications are well established theoretically. Thus the region in which

the ion cyclotron waves are observed is the plasma depletion layer (1303–1340 UT), which is between the magnetopause ($\sim$ 1300 UT) and the magnetosheath proper (1340–1400 UT), where mirror fluctuations are primarily observed.

In order to demonstrate that the spatial ordering magnetopause–ion cyclotron waves–mirror mode holds in general for the high magnetosheath beta conditions during which AMPTE/CCE observes the magnetosheath, Anderson and Fuselier [1993] made a statistical study of transitions from magnetopause crossings and from time intervals with ion cyclotron or mirror mode fluctuations. The results are shown in Table 1 (adapted from [*Anderson and Fuselier*, 1993]). Transitions are shown to magnetopause crossings and to time intervals with ion cyclotron, mirror mode, or "other sheath" waves. "Other sheath" indicates intervals in which the waves are broadband (structureless) fluctuations extending above Ω_p, or some combination of ion cyclotron fluctuations and mirror mode fluctuations not considered in [*Anderson and Fuselier*, 1993] (see below). Most of the magnetopause transitions are to ion cyclotron intervals. About half of the transitions from ion cyclotron waves are to the magnetopause, while the other half are to intervals with mirror mode or "other sheath" waves. None of the mirror mode transitions are to the magnetopause. Therefore, it is clear that there is a spatial ordering with the positions corresponding to ion cyclotron fluctuations close to the magnetopause while the positions corresponding to the mirror mode are farther away.

Anderson and Fuselier [1993] distinguished three types of magnetic fluctuation spectra. These were ion cyclotron waves with transverse fluctuations and with ω_r extending above the alpha particle gyrofrequency $\Omega_\alpha \sim 0.5\Omega_p$, low frequency transverse fluctuations with $\omega_r < \Omega_\alpha$ (which we now recognize as lower frequency ion cyclotron waves), and the mirror mode. Recently, Anderson et al. [1993] have provided a more complete categorization by distinguishing five different categories of fluctuation spectra bounded above by the proton cyclotron frequency.

Examples of spectral power density versus normalized wave frequency, ω_r/Ω_p, are shown for each of these spectral categories in Figure 2 (which is taken from [*Anderson et al.*, 1993]). In the Figure, the left hand polarized transverse (to $\mathbf{B_0}$) power density is indicated by the solid curve, while the right hand transverse and parallel power density are indicated by the dotted and dashed lines respectively. (Note that the peak at very low frequency, $\omega_r \sim 0.05\Omega_p$ which occurs in the

BIF, CON, and LOW spectra is a numerical artifact, and should be ignored.) The characteristics of the spectral categories are:

[1] Bifurcated (BIF, or B — the three letter abbreviations are used in Figure 2, while the one letter abbreviations are used in Figure 4) transverse spectra with two peaks in wave power, and a clearly resolved gap between the two. The higher frequency peak may extend above the alpha particle gyrofrequency, Ω_α, while the lower frequency peak is entirely below Ω_α.

[2] Continuous (CON, or C) transverse spectra having a single peak in wave power with frequency width extending above Ω_α.

[3] Low frequency transverse (Low, or L) spectra with a single maximum at a frequency below Ω_α and with no significant energy at frequencies above Ω_α.

[4] Mirror plus low frequency transverse (MRL, or L and M) spectra in which the mirror-like longitudinal fluctuations and low frequency transverse fluctuations are both present at different frequencies.

[5] Mirror (MIR, or M) spectra with predominantly longitudinal magnetic fluctuations, spectral maxima at $\omega_r \sim \Omega_\alpha$, and no transverse components above the noise level.

There is in fact a continuous transition between these types, so the differences between the observed spectra in adjacent categories may be small, but the differences between non-adjacent categories are significant.

The different spectral types occur at different values of plasma beta. We characterize the plasma beta using the parallel proton beta, $\beta_{\|p}$, which we define in this paper as the ratio of the parallel pressure and the magnetic pressure,

$$\beta_{\|p} \equiv 8\pi n_p T_{\|p}/(3B_0^2), \tag{1}$$

with n_p and $T_{\|p}$ being the proton density and temperature parallel to $\mathbf{B_0}$ respectively. Figure 3, taken from [*Anderson et al.*, 1993], shows 102 wave events plotted in A_p, $\beta_{\|p}$ space, where A_p is the proton temperature anisotropy,

$$A_p \equiv (T_\perp / T_\|)_p - 1. \tag{2}$$

Each wave event represents from 5 to 30 minutes of data (see [*Anderson et al.*, 1993] for more details). In the upper left panel, all the events are plotted together, while in the five remaining

panels, the events are plotted separately by category (BIF, CON, etc).

Note from the upper left panel of Figure 3 that all the events lie along a straight line, which Anderson et al. [1993] have fit to $A_p = 0.50\beta_{\|p}^{-0.48}$ (the solid line in the Figure). The events lie along this line because it is close to the marginal stability condition for ion cyclotron and mirror mode waves [*Gary et al.*, 1993a; *Denton et al.*, 1993a; *Gary and Winske*, 1993; *Gary et al.*, 1993b]. Though the magnetosheath plasma convects through the plasma depletion layer, and the plasma parameters corresponding to a particular moving flux tube are continually changing, Denton et al. [1993a] has shown that the local instability has sufficient time to saturate nonlinearly and reduce the anisotropy, so that the plasma is near marginal stability. Therefore, the plasma depletion layer is in a driven, time independent state. The dashed curve in the upper left panel of Figure 3 shows the contour in A_p - $\beta_{\|p}$ space for which the proton cyclotron (driven by the proton anisotropy) growth rate is equal to $0.01\Omega_p$, while the dotted line shows the corresponding curve for the mirror mode. Note how these contours parallel the data values.

The remaining panels showing wave events separated by spectral category demonstrate clearly that the spectral type of the observed waves is ordered by $\beta_{\|p}$, with the lowest values of $\beta_{\|p}$ corresponding to bifurcated (BIF) events, while the largest values of $\beta_{\|p}$ correspond to mirror mode (MIR) events. The events with the mirror mode exclusively (MIR) generally have values of $\beta_{\|p}$ for which the contour of constant growth rate for the mirror mode (the dotted line) lies below that for the proton cyclotron mode (the dashed line) [*Gary et al.*, 1993a], so that the mirror mode growth rate is larger.

Since variation of $\beta_{\|p}$ is strongly related to the spatial structure across the plasma depletion layer, the fact that the spectral wave types are ordered by $\beta_{\|p}$ indicates that the variation of spectral type relates to the spatial variation of $\beta_{\|p}$ across the plasma depletion layer and into the magnetosheath proper. Thus the bifurcated (BIF) category occurs close to the magnetopause, while the mirror mode (MIR) occurs more often in the magnetosheath proper.

Denton et al. [1993a] showed theoretically that the detailed frequency spectrum of waves could be explained in the case of one event with a bifurcated (BIF) spectrum. Subsequently, Denton et al. [1993b] extended their analysis of the frequency spectrum to the full range of plasma depletion layer and magnetosheath conditions. They introduced a model for the plasma variation across the

plasma depletion layer and into the magnetosheath proper (the model is similar to that of [*Gary et al.*, 1993a; *Gary and Winske*, 1993; *Gary et al.*, 1993b]). The model incorporates anisotropic protons and alpha particles (at 4% of the proton density with $(T_\perp/T_\parallel)_\alpha = 1.3(T_\perp/T_\parallel)_p$) and isotropic electrons (see [*Denton et al.*, 1993b] for details). The central feature of the model is the anisotropy-beta relation discussed above, $A_p = 0.50\beta_{\parallel p}^{-0.48}$.

Figure 4 (taken from *Denton et al.* [1993b]) shows how the variation of the observed fluctuation spectra follows naturally from the magnetosheath and plasma depletion layer model. At each value of $\beta_{\parallel p}$ (plotted on the horizontal axis), the model has been used to generate the plasma parameters. Panel (a) shows the normalized frequency range (ω_r/Ω_p) of ion cyclotron instability using the full model, while panel (b) shows the result with A_α lowered to zero, and panel (c) shows the result with A_p lowered to zero. The solid lines indicate frequency values corresponding to marginal stability, while the long and short dashed lines are plotted at frequencies corresponding to maxima in the growth rate. We note from panel (a) that at low $\beta_{\parallel p}$ there are two regions of instability, one with frequency above Ω_α, and one with frequency below. These regions of instability merge at $\beta_{\parallel p}$ slightly less than unity. Panels (b) and (c) show clearly that the higher frequency mode is driven by the anisotropy of the protons, while the lower frequency mode is driven by the anisotropy of the alpha particles. Thus we identify the higher frequency mode as the proton cyclotron mode and the lower frequency mode as the alpha cyclotron mode (indicated by the letters p and α in the Figure). Panel (d) shows the normalized temporal growth rate, γ/Ω_p, for the higher frequency proton cyclotron mode (long dashes), lower frequency alpha cyclotron mode (shorter dashes), and the mirror mode (solid line), using the full model. Panels (e) and (f) have $A_\alpha = 0$ and $A_p = 0$ respectively. Note from panel (d) that the mirror mode growth rate becomes larger than the ion cyclotron mode growth rates at $\beta_{\parallel p} \sim 6$.

The letters B, C, L, L over M, and M in panel (a) of Figure 4 refer to the spectral categories discussed above. Each one of these letters is plotted at a horizontal position which corresponds to the average value of $\beta_{\parallel p}$ for the events in that category in the study of [*Anderson et al.*, 1993]. We see that B is plotted where the model predicts a bifurcated spectrum of ion cyclotron waves, C and L are plotted where the model predicts a merged spectrum, L over M is plotted where the mirror mode growth rate starts to become significant, and M is plotted where the mirror mode

growth rate becomes greater than that of the ion cyclotron modes. Thus the $\beta_{\|p}$ variation of spectral properties is well predicted by the theory. In fact, there is a remarkable resemblance between Figure 1 and Figure 4 because the passage of the satellite shown in Figure 1 corresponds to passage into the plasma depletion layer and into the magnetosheath where $\beta_{\|p}$ becomes larger. As further evidence of the adequacy of linear Vlasov theory to predict the wave properties, the unstable frequency bands for the example cases are shown in Figure 2 as horizontal bars: again there is good agreement, except for the mirror mode (MIR) case, for which the theory predicts ion cyclotron waves. Possibly, presence of the mirror mode inhibits the ion cyclotron mode in this case.

The fact that the proton and alpha cyclotron instabilities approach their respective gyrofrequencies at low $\beta_{\|p}$ is easy to understand. Instability occurs for particles which are Doppler shifted up to their gyrofrequency. At low $\beta_{\|p}$, the thermal velocity is small compared to the Alfvén speed, which is roughly equal to the phase velocity of the waves. So at low $\beta_{\|p}$, the wave frequency must approach the gyrofrequency. At higher $\beta_{\|p}$, the Doppler shift is greater, hence the wave frequency is lower.

The data presented here pertain only to periods with high solar wind dynamic pressure, i.e. high magnetosheath beta. For low dynamic pressure conditions the beta just downstream of the bow shock may be quite low, ~ 1. In this case, the magnetosheath plasma will evolve along the same A_p, $\beta_{\|p}$ relation obtained here as it convects toward the magnetopause, but will start on the curve at a lower value of $\beta_{\|p}$ and higher value of A_p than the high beta cases studied to date. Hence, under these conditions it is possible that ion cyclotron waves could dominate the observed spectrum throughout the magnetosheath [Sckopke et al., 1990], so that the mirror mode is not observed. Such a result is entirely consistent with the results stated here provided that the low beta plasma in the magnetosheath is highly anisotropic (see Figure 3). Indeed, highly anisotropic proton distributions have been observed downstream of low beta shocks [*Thomsen et al.*, 1985; Sckopke et al., 1990]. While distributions downstream of low beta shocks are much more anisotropic than the distributions observed in the high beta magnetosheath proper by AMPTE/CCE, it is important to realize that they still only represent a plasma that is marginally stable to the growth of ion cyclotron waves.

We have shown that the low frequency waves ($\omega_r \leq \Omega_p$) observed by AMPTE/CCE in the plasma depletion layer and magnetosheath proper are well identified with proton cyclotron waves (driven by A_p), alpha cyclotron waves (driven by A_α), and the mirror mode. The wave spectral properties are well ordered with respect to the proton parallel beta, $\beta_{\|p}$. Such a result is predicted by linear Vlasov theory using a simple model for the plasma depletion layer. Because of this, the observed spectral type is related to relative distance from the magnetopause, since $\beta_{\|p}$ increases sharply away from the magnetopause within the plasma depletion layer and into the magnetosheath proper. The anisotropy–beta relation, $A_p = 0.50\beta_{\|p}^{-0.48}$, results from the fact that the waves pitch angle scatter the particles so that the plasma is near marginal stability. This relation supplies a fundamental constraint on the plasma, and should be taken into account in fluid descriptions of the plasma depletion layer and magnetosheath proper.

Acknowledgments. The work at Dartmouth has been supported with funding from NASA under grants NAGW-1652 and NA 5-1098. Work at the Johns Hopkins University Applied Physics Laboratory was supported by NASA under the AMPTE Missions Operations and Data Analysis program. Research at Lockheed Palo Alto Research Laboratory was funded through NASA contract NAS5-30565 and the NASA Guest Investigator program NAS5-31213. The Los Alamos portion of this work was performed under the auspices of the U.S. Department of Energy (DOE) and was supported by the DOE Office of Basic Energy Sciences, Division of Engineering and Geosciences, and the SR&T Program of the National Aeronautics and Space Administration (NASA). We also acknowledge a grant of computer time from NCSA.

REFERENCES

Anderson, B.J., S.A. Fuselier, and D. Murr, Electromagnetic ion cyclotron waves observed in the plasma depletion layer, *Geophys. Res. Lett.*, 18, No. 11, 1955–1958, 1991.

Anderson, B.J. and S.A. Fuselier, Magnetic pulsations from 0.1 to 4.0 Hz and associated plasma properties in the Earth's subsolar magnetosheath and plasma depletion layer, *J. Geophys. Res.*, 98, 1461–1479, 1993.

Anderson, B.J., S.A. Fuselier, S.P. Gary, and R.E. Denton, Magnetic Spectral Signatures from 0.1 to 4.0 Hz in the Earth's Magnetosheath and Plasma Depletion Layer, submitted to *J. Geophys. Res.*, 1993.

Crooker, N.U., T.E. Eastman, and G.S. Stiles, Observations of plasma depletion in the magnetosheath at the dayside magnetopause, *J. Geophys. Res.*, 84, No. A3, 869–874, 1979.

Denton, R.E., M.K. Hudson, S.A. Fuselier, and B.J. Anderson, Electromagnetic ion cyclotron waves in the plasma depletion layer, *J. Geophys. Res.*, in press, 1993a.

Denton, R.E. S.P. Gary, B.J. Anderson, S.A. Fuselier, and M.K. Hudson, Low-frequency magnetic fluctuation spectra in the magnetosheath and plasma depletion layer, to be submitted to *J. Geophys. Res.*, 1993b.

Fuselier, S.A., D.M. Klumpar, E.G. Shelley, B.J. Anderson, and A.J. Coates, He^{2+} and H^{+} dynamics in the subsolar magnetosheath and plasma depletion layer, *J. Geophys. Res.*, 96, No. A12, 21095–21104, 1991.

Energetic magnetospheric protons in the plasma depletion layer, *J. Geophys. Res.*, 97, 13759, 1992.

Gary, S.P., M.D. Montgomery, W.C. Feldman, and D.W. Forslund, Proton temperature anisotropy instabilities in the solar wind, *J. Geophys. Res.*, 81, No. 7, 1241–1246, 1976.

Gary, S.P., S.A. Fuselier, and B.J. Anderson, Ion anisotropy instabilities in the magnetosheath, *J. Geophys. Res.*, 98, 1481–1488, 1993a.

Gary, S.P. and D. Winske, Simulations of ion cyclotron anisotropy instabilities in the terrestrial magnetosheath, *J. Geophys. Res.*, in press, 1993.

Gary, S.P., B.J. Anderson, R.E. Denton, S A. Fuselier, M.E. McKean, and D. Winske, ELVIS lives (!) in the magnetosheath, submitted to *Geophys. Res. Lett.*, 1993b.

Lees, L.C., Interaction between the solar plasma wind and the geomagnetic cavity, *AIAA J.*, 2, 2065, 1964.

Midgley, J.E. and L. Davis, Calculation by a moment technique of the perturbation of the geomagnetic field by the solar wind, *J. Geophys. Res.*, 68, 5111, 1963.

Sckopke, N., G. Paschmann, A. L. Brinca, C. W. Carlson, and H. Luhr, Ion thermalization in quasi-perpendicular shocks involving reflected ions, *J. Geophys. Res.*, 95, 6337, 1990.

Thomsen, M.F., J.T. Gosling, S.J. Bame, and M.M. Mellott, Ion and electron heating at collisionless shocks near the critical mach number, *J. Geophys. Res.*, 90, 137-148, 1985.

Wu, C.C., MHD flow past an obstacle: large-scale flow in the magnetosheath, *Geophys. Res. Lett.*, 19, No. 2, 87–90, 1992.

Zwan, B.J. and R.A. Wolf, Depletion of solar wind plasma near a planetary boundary, 81, No. 10, 1636–1648, 1976.

FIGURE CAPTIONS

Table 1. Percentage of transitions from the magnetopause and from time intervals during which ion cyclotron and mirror mode waves were observed, to the magnetopause or to time intervals with ion cyclotron, mirror mode, or "other sheath" (see text) waves. For each of the categories from which transitions occur, the number of total transitions is indicated as "No. Events".

Fig. 1. Dynamic spectra of AMPTE/CCE magnetic field data together with CCE and IRM density and magnetic field data. The top panel (labeled "XY") shows the transverse (to $\mathbf{B_0}$) spectral power from 0 to 2 Hz and the second panel (labeled "Z") shows the parallel power over the same frequency range. The third panel shows the electron density at CCE, calculated as the sum of the proton density and twice the He2+ density measured by the HPCE instrument. The IRM electron density, measured by the electron instrument was multiplied by 4.92, determined as the ratio between the densities from 1340 to 1400 UT. The IRM time has been shifted by 3.5 minutes to account for the plasma convection from IRM to CCE. The bottom panel shows the CCE and IRM magnetic field strength, B_0. The IRM field magnitude was multiplied by 4.81, the ratio obtained from the 1340-1400 UT interval.

Fig. 2. Example power spectra of magnetic field data for the five spectral categories of [*Anderson et al.*, 1993] defined in the text. Left and right hand polarized power in the plane perpendicular to $\mathbf{B_0}$ are indicated by the solid and dotted curves respectively, while the power of fluctuations parallel to $\mathbf{B_0}$ is indicated by the dashed curve. The horizontal bars above the spectra show the frequency range of linear instability predicted by Vlasov theory.

Fig. 3. Plot of proton temperature anisotropy, A_p versus parallel proton beta, $\beta_{\|p}$, for all the events in the study of [*Anderson et al.*, 1993] (upper left panel), and for the events in each spectral category individually. The solid line in the upper left panel shows the least squares fit relation: $A_p = 0.50\beta_{\|p}^{-0.48}$. The dashed curve shows the contour of proton cyclotron growth rate of $0.015\Omega_p$ and the dotted curve shows the corresponding contour for the mirror mode assuming 4% He^{2+}.

Fig. 4. Properties of the ion cyclotron anisotropy instabilities and the mirror instability as functions of $\beta_{\|p}$ under the parameters of the model of [*Denton et al.*, 1993b]. The top three panels illustrate frequencies ω_r which are relevant to the ion cyclotron anisotropy instabilities; the solid lines indicate the frequencies which bound the instability regimes, $\gamma/\Omega_p = 1 \times 10^{-4}$, and the dashed lines indicate the frequencies which correspond to a local maximum (with respect to ω_r) in temporal growth rate, γ. The bottom three panels illustrate the maximum growth rates for the proton cyclotron instability (the long dashed lines),

the helium cyclotron instability (the short dashed lines), and the mirror instability (the solid lines). Panels (a) and (d) correspond to the full model. Panels (b) and (e) represent results from the model except that $(T_\perp/T_\parallel)_\alpha = 1.0$, and panels (c) and (f) represent results from the model except that $(T_\perp/T_\parallel)_p = 1.0$. The letters B, C, L, L over M, and M in panel (a) indicate the spectral categories of [*Anderson et al.*, 1993] defined in the text. They are plotted at a horizontal position corresponding to the average value of $\beta_{\parallel p}$ for the events in each category.

Transitions From:	No. Events	to MgPause	to Ion Cyc.	to Mirror	to Other Sheath
MgPause	30	—	77%	0%	23%
Ion Cyc.	36	64%	—	19%	17%
Mirror	18	0%	50%	—	50%

Table 1

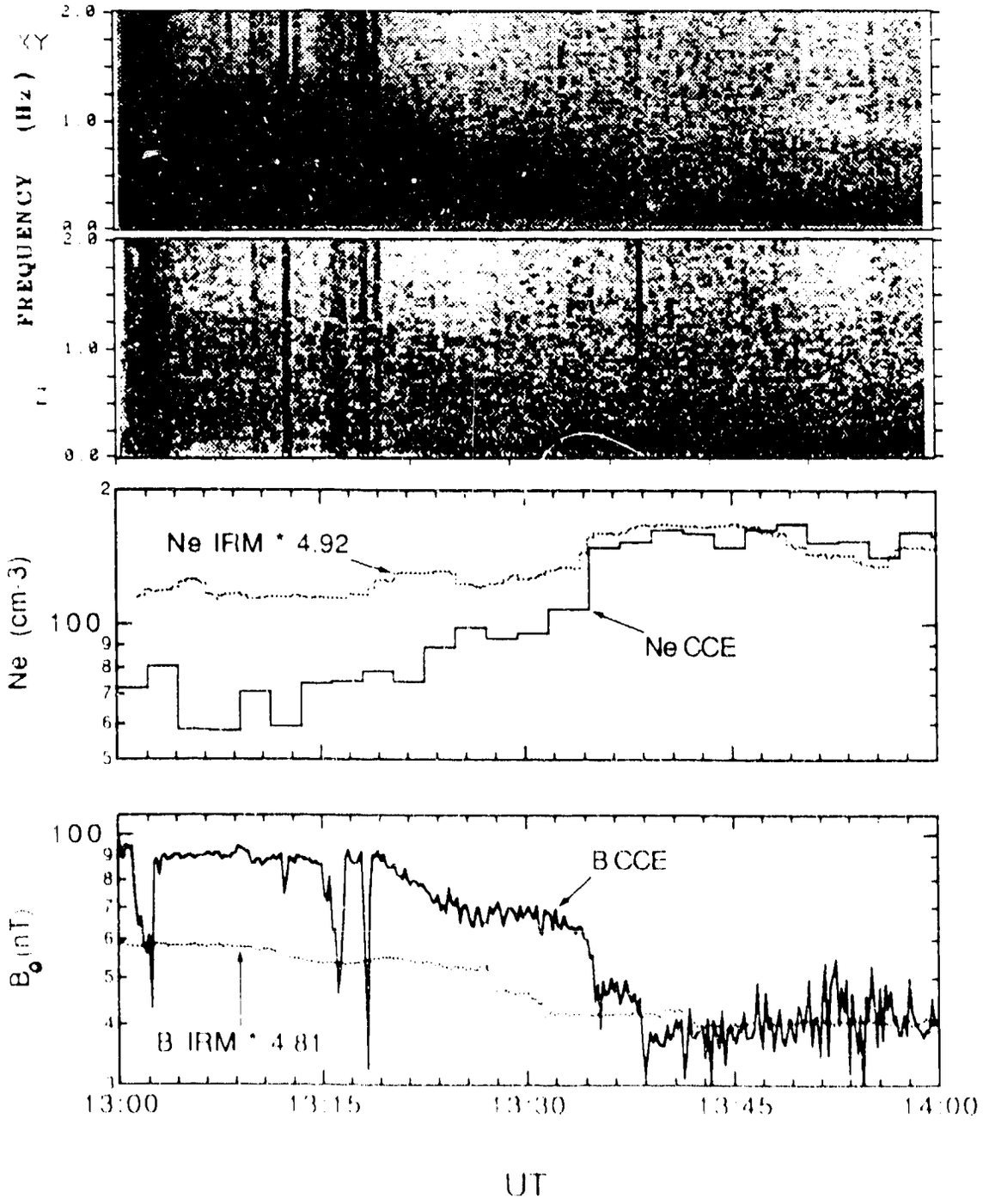
FREQUENCY (Hz)
XY
2.0
1.0
0.0
Ne (cm-3)
Ne IRM * 4.92
Ne CCE
100
B CCE
B IRM * 4.81
13:00
13:15
13:30
13:45
14:00
UT

Fig 1

Example Power Spectra: AMPTE/CCE 1984 Day 280

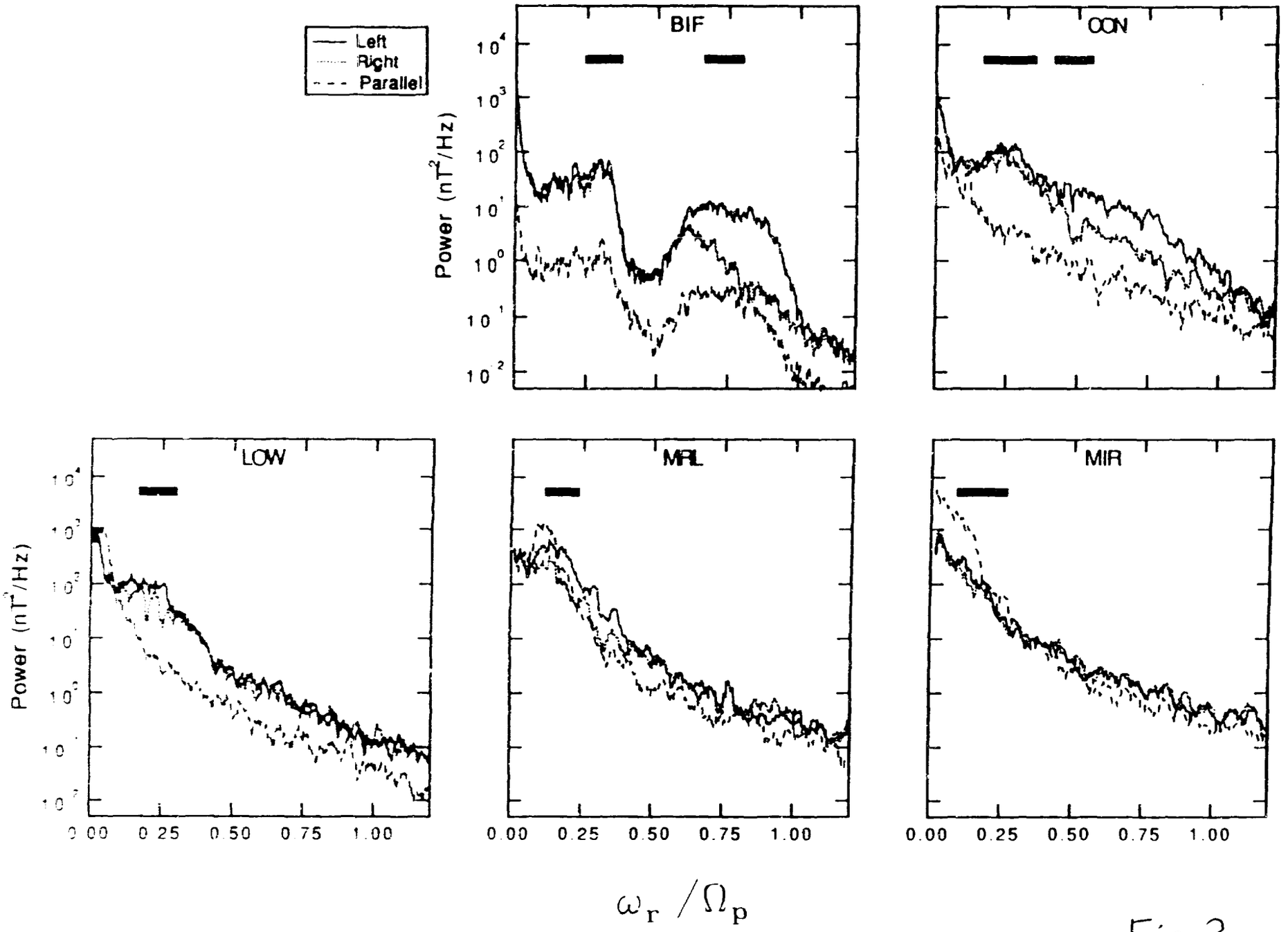

Fig 2

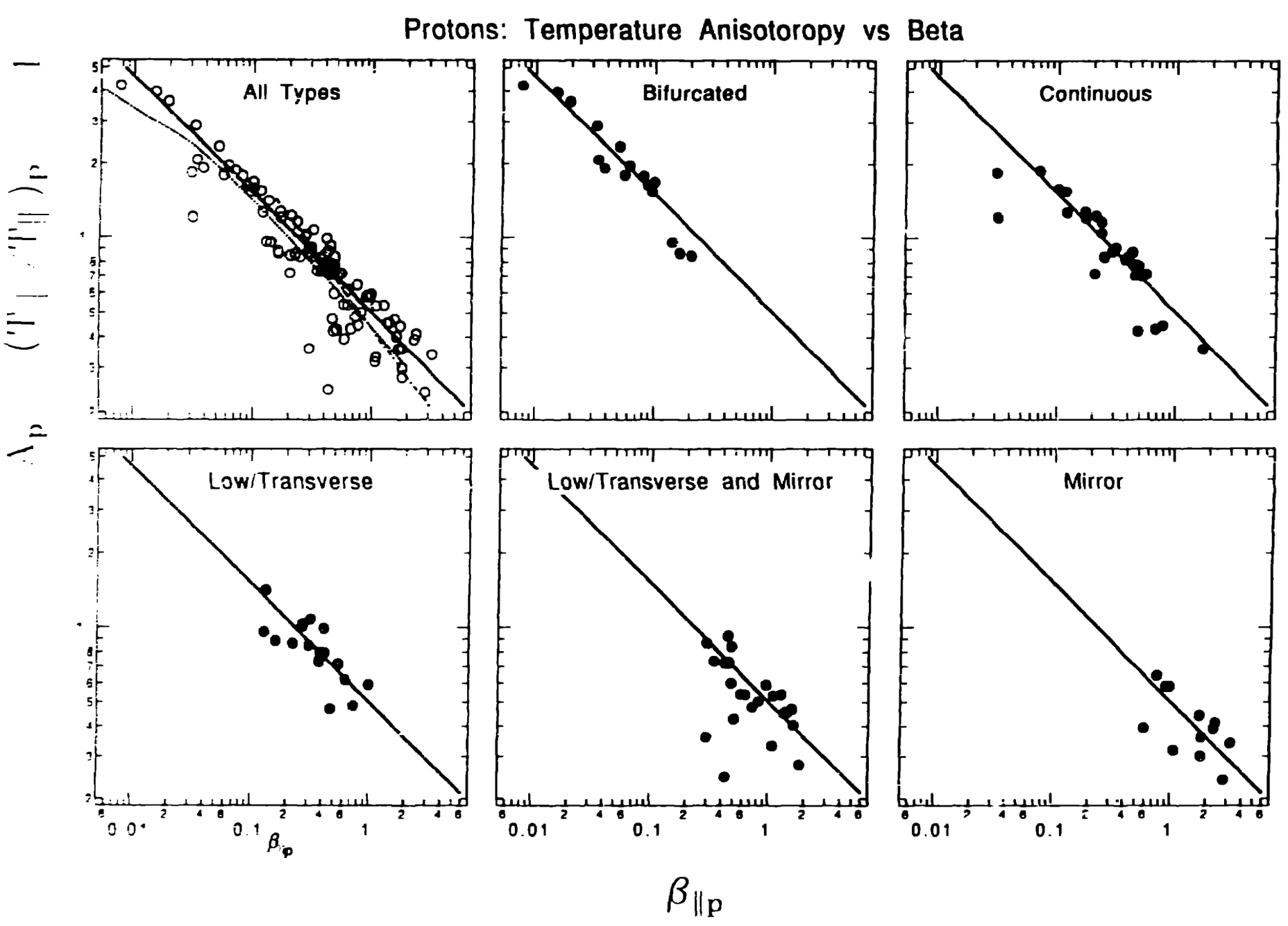
Protons: Temperature Anisotoropy vs Beta
All Types
Bifurcated
Continuous
Low/Transverse
Low/Transverse and Mirror
Mirror
0.01
0.1
1
$\beta_{\|p}$

Fig 3

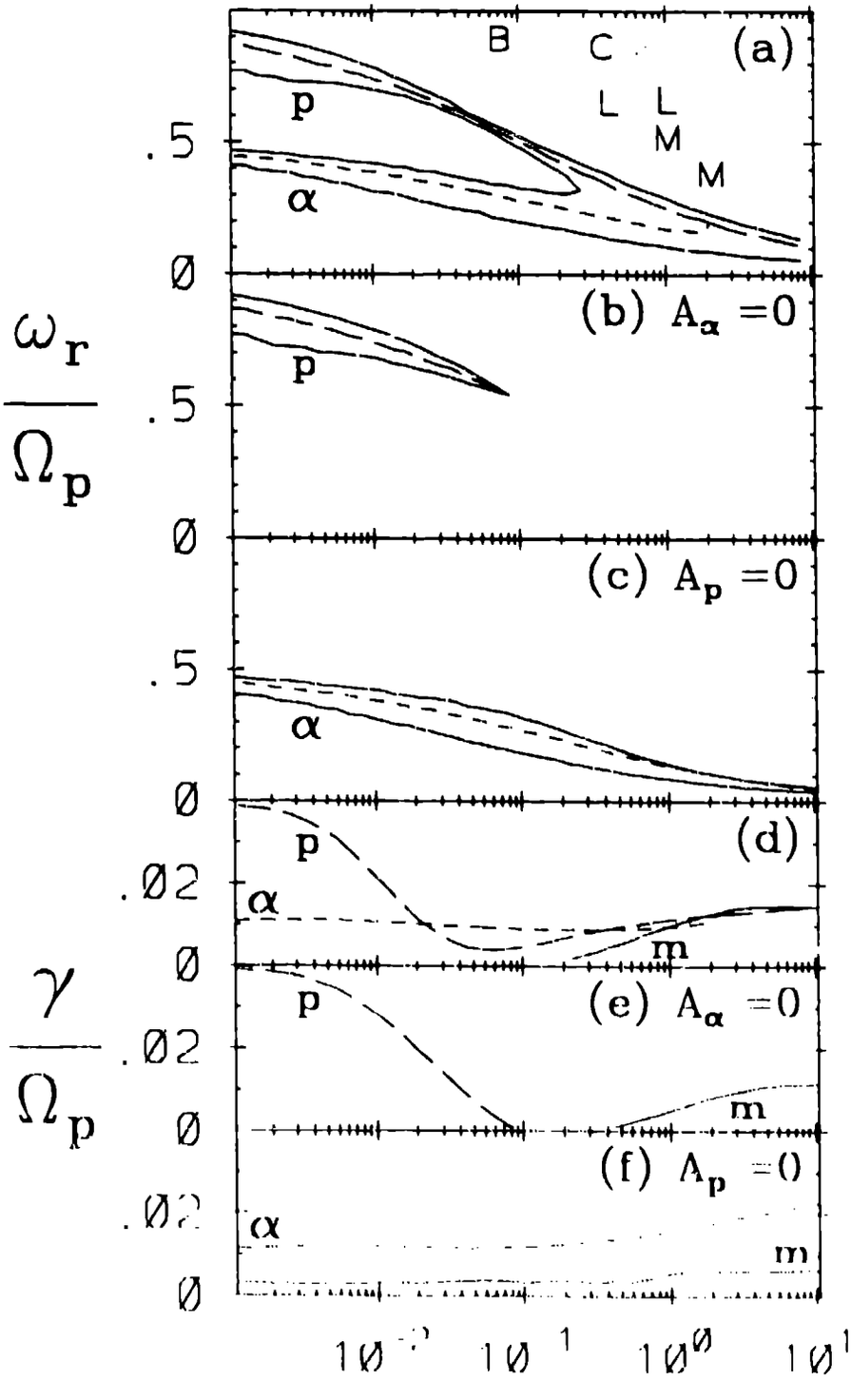
B
C
(a)
L L
M
M
p
α
.5
Ø
(b) A_α =0
p
.5
Ø
(c) A_p =0
.5
α
Ø
(d)
p
.Ø2
α
Ø
m
(e) A_α =0
p
.Ø2
Ø
m
(f) A_p =0
.Ø2
α
m
Ø
$\frac{\omega_r}{\Omega_p}$
$\frac{\gamma}{\Omega_p}$
10^{-2}
10^{-1}
10^{0}
10^{1}
$\beta_{\|p}$

Fig. 4